Research Article | Vol. 25, No. 12 | 12 Jun 2017 | OPTICS EXPRESS 13705
Optics EXPRESS

Ultra-narrow-linewidth $Al_2O_3:Er^{3+}$ lasers with a wavelength-insensitive waveguide design on a wafer-scale silicon nitride platform

PURNAWIRMAN,[1] NANXI LI,[1,2,*] EMIR SALIH MAGDEN,[1] GURPREET SINGH,[1] NEETESH SINGH,[1] ANNA BALDYCHEVA,[1] EHSAN SHAH HOSSEINI,[1] JIE SUN,[1] MICHELE MORESCO,[1] THOMAS N. ADAM,[3] GERARD LEAKE,[3] DOUGLAS COOLBAUGH,[3] JONATHAN D. B. BRADLEY,[1,4] AND MICHAEL R. WATTS[1]

[1]*Research Laboratory of Electronics, Massachusetts Institute of Technology, Cambridge, MA 02139, USA*
[2]*John A. Paulson School of Engineering and Applied Science, Harvard University, Cambridge, MA 02138, USA*
[3]*College of Nanoscale Science and Engineering, University at Albany, Albany, New York 12203, USA*
[4]*Current address: Department of Engineering Physics, McMaster University, 1280 Main Street West, Hamilton, Ontario L8S 4L7, Canada*
[*]*nanxili@mit.edu*

Abstract: We report ultra-narrow-linewidth erbium-doped aluminum oxide ($Al_2O_3:Er^{3+}$) distributed feedback (DFB) lasers with a wavelength-insensitive silicon-compatible waveguide design. The waveguide consists of five silicon nitride (SiN_x) segments buried under silicon dioxide (SiO_2) with a layer $Al_2O_3:Er^{3+}$ deposited on top. This design has a high confinement factor (> 85%) and a near perfect (> 98%) intensity overlap for an octave-spanning range across near infra-red wavelengths (950–2000 nm). We compare the performance of DFB lasers in discrete quarter phase shifted (QPS) cavity and distributed phase shifted (DPS) cavity. Using QPS-DFB configuration, we obtain maximum output powers of 0.41 mW, 0.76 mW, and 0.47 mW at widely spaced wavelengths within both the C and L bands of the erbium gain spectrum (1536 nm, 1566 nm, and 1596 nm). In a DPS cavity, we achieve an order of magnitude improvement in maximum output power (5.43 mW) and a side mode suppression ratio (SMSR) of > 59.4 dB at an emission wavelength of 1565 nm. We observe an ultra-narrow linewidth of $\Delta\nu_{DPS}$ = 5.3 ± 0.3 kHz for the DPS-DFB laser, as compared to $\Delta\nu_{QPS}$ = 30.4 ± 1.1 kHz for the QPS-DFB laser, measured by a recirculating self-heterodyne delayed interferometer (R-SHDI).

OCIS codes: (130.0130) Integrated optics; (130.3120) Integrated optics devices; (140.3460) Lasers; (130.2790) Guided waves.

References and links

1. C. Spiegelberg, J. Geng, Y. Hu, Y. Kaneda, S. Jiang, and N. Peyghambarian, "Low-noise narrow-linewidth fiber laser at 1550 nm (June 2003)," J. Lightwave Technol. **22**(1), 57–62 (2004).
2. B. R. Koch, A. W. Fang, E. Lively, R. Jones, O. Cohen, D. J. Blumenthal, and J. E. Bowers, "Mode locked and distributed feedback silicon evanescent lasers," Laser Photonics Rev. **3**(4), 355–369 (2009).
3. N. Kobayashi, K. Sato, M. Namiwaka, K. Yamamoto, S. Watanabe, T. Kita, H. Yamada, and H. Yamazaki, "Silicon photonic hybrid ring-filter external cavity wavelength tunable lasers," J. Lightwave Technol. **33**(6), 1241–1246 (2015).
4. C. T. Santis, S. T. Steger, Y. Vilenchik, A. Vasilyev, and A. Yariv, "High-coherence semiconductor lasers based on integral high-Q resonators in hybrid Si/III-V platforms," in *Proceedings of the National Academy of Sciences,* **111**, pp. 2879–2884, February 2014.
5. E. H. Bernhardi, H. A. G. M. van Wolferen, L. Agazzi, M. R. H. Khan, C. G. H. Roeloffzen, K. Wörhoff, M. Pollnau, and R. M. de Ridder, "Ultra-narrow-linewidth, single-frequency distributed feedback waveguide laser in $Al_2O_3:Er^{3+}$ on silicon," Opt. Lett. **35**(14), 2394–2396 (2010).

#286500 https://doi.org/10.1364/OE.25.013705
Journal © 2017 Received 16 Feb 2017; revised 21 Apr 2017; accepted 18 May 2017; published 8 Jun 2017

Optics EXPRESS

6. Purnawirman, J. Sun, T. N. Adam, G. Leake, D. Coolbaugh, J. D. B. Bradley, E. S. Hosseini, and M. R. Watts, "C- and L-band erbium-doped waveguide lasers with wafer-scale silicon nitride cavities," Opt. Lett. **38**(11), 1760–1762 (2013).
7. M. Belt and D. J. Blumenthal, "Erbium-doped waveguide DBR and DFB laser arrays integrated within an ultra-low-loss Si_3N_4 platform," Opt. Express **22**(9), 10655–10660 (2014).
8. E. S. Hosseini, Purnawirman, J. D. B. Bradley, J. Sun, G. Leake, T. N. Adam, D. Coolbaugh, and M. R. Watts, "CMOS-compatible 75 mW erbium-doped distributed feedback laser," Opt. Lett. **39**(11), 3106–3109 (2014).
9. M. Belt, T. Huffman, M. L. Davenport, W. Li, J. S. Barton, and D. J. Blumenthal, "Arrayed narrow linewidth erbium-doped waveguide-distributed feedback lasers on an ultra-low-loss silicon-nitride platform," Opt. Lett. **38**(22), 4825–4828 (2013).
10. Purnawirman, E. S. Hosseini, A. Baldycheva, J. Sun, J. D. B. Bradley, T. N. Adam, G. Leake, D. Coolbaugh, and M. R. Watts, "Erbium-doped laser with multi-segmented silicon nitride structure," in *Proceedings of the 2014 Optical Fiber Communications Conference and Exhibition (OFC),* (2014).
11. G. Singh, Purnawirman, J. D. B. Bradley, N. Li, E. S. Magden, M. Moresco, T. N. Adam, G. Leake, D. Coolbaugh, and M. R. Watts, "Resonant pumped erbium-doped waveguide lasers using distributed Bragg reflector cavities," Opt. Lett. **41**(6), 1189–1192 (2016).
12. N. Li, Z. Purnawirman, Z. Su, E. S. Magden, P. T. Callahan, K. Shtyrkova, M. Xin, A. Ruocco, C. Baiocco, E. P. Ippen, F. X. Kärtner, J. D. B. Bradley, D. Vermeulen, and M. R. Watts, "High-power thulium lasers on a silicon photonics platform," Opt. Lett. **42**(6), 1181–1184 (2017).
13. A. Gondarenko, J. S. Levy, and M. Lipson, "High confinement micron-scale silicon nitride high Q ring resonator," Opt. Express **17**(14), 11366–11370 (2009).
14. Z. Su, N. Li, E. S. Magden, M. Byrd, Purnawirman, T. N. Adam, G. Leake, D. Coolbaugh, J. D. B. Bradley, and M. R. Watts, "Ultra-compact and low-threshold thulium microcavity laser monolithically integrated on silicon," Opt. Lett. **41**(24), 5708–5711 (2016).
15. C. V. Poulton, M. J. Byrd, M. Raval, Z. Su, N. Li, E. Timurdogan, D. Coolbaugh, D. Vermeulen, and M. R. Watts, "Large-scale silicon nitride nanophotonic phased arrays at infrared and visible wavelengths," Opt. Lett. **42**(1), 21–24 (2017).
16. K. Tada, Y. Nakano, and A. Ushirokawa, "Proposal of a distributed feedback laser with nonuniform stripe width for complete single-mode oscillation," Electron. Lett. **20**(2), 82–84 (1984).
17. J. W. Dawson, N. Park, and K. J. Vahala, "An improved delayed self-heterodyne interferometer for linewidth measurements," IEEE Photonics Technol. Lett. **4**(9), 1063–1066 (1992).
18. N. Li, E. Timurdogan, C. V. Poulton, M. Byrd, E. S. Magden, Z. Su, Purnawirman, G. Leake, D. Coolbaugh, D. Vermeulen, and M. R. Watts, "C-band swept wavelength erbium-doped fiber laser with a high-Q tunable interior-ridge silicon microring cavity," Opt. Express **24**(20), 22741–22748 (2016).
19. H. Abe, S. G. Ayling, J. H. Marsh, R. M. Delarue, and J. S. Roberts, "Single-mode operation of a surface grating distributed-feedback GaAs-AlGaAs laser with variable-width waveguide," IEEE Photonics Technol. Lett. **7**(5), 452–454 (1995).
20. M. Okai, "Spectral characteristics of distributed-feedback semiconductor-lasers and their improvements by corrugation-pitch-modulated structure," J. Appl. Phys. **75**(1), 1–29 (1994).
21. J. D. B. Bradley, Z. Su, E. S. Magden, N. Li, M. Byrd, Purnawirman, T. N. Adam, G. Leake, D. Coolbaugh, and M. R. Watts, "1.8-μm thulium microlasers integrated on silicon," Proc. SPIE **9744**, 97440U (2016).
22. Purnawirman, N. Li, E. S. Magden, G. Singh, M. Moresco, T. N. Adam, G. Leake, D. Coolbaugh, J. D. B. Bradley, and M. R. Watts, "Wavelength division multiplexed light source monolithically integrated on a silicon photonics platform," Opt. Lett. **42**(9), 1772–1775 (2017).
23. N. Li, Z. Su, Purnawirman, E. S. Magden, C. V. Poulton, A. Ruocco, N. Singh, M. J. Byrd, J. D. B. Bradley, G. Leake, and M. R. Watts, "Athermal synchronization of laser source with WDM filter in a silicon photonics platform," Appl. Phys. Lett. **110**(21), 211105 (2017).
24. S. S. Sui, M. Y. Tang, Y. D. Yang, J. L. Xiao, Y. Du, and Y. Z. Huang, "Sixteen-Wavelength Hybrid AlGaInAs/Si Microdisk Laser Array," IEEE J. Quantum Electron. **51**, 2600108 (2015).
25. S. Tanaka, S. H. Jeong, S. Sekiguchi, T. Akiyama, T. Kurahashi, Y. Tanaka, and K. Morito, "Four-wavelength silicon hybrid laser array with ring-resonator based mirror for efficient CWDM transmitter," in *2013 Optical Fiber Communication Conference and Exposition and the National Fiber Optic Engineers Conference (OFC/NFOEC)*, 2013, OTh1D3.
26. S. Tanaka, S.-H. Jeong, S. Sekiguchi, T. Kurahashi, Y. Tanaka, and K. Morito, "High-output-power, single-wavelength silicon hybrid laser using precise flip-chip bonding technology," Opt. Express **20**(27), 28057–28069 (2012).
27. S.-H. Jeong, S. Tanaka, S. Sekiguchi, T. Kurahashi, N. Hatori, S. Akiyama, T. Usuki, T. Yamamoto, T. Akiyama, Y. Tanaka, and K. Morito, "Silicon-wire waveguide based external cavity laser for milliwatt-order output power and temperature control free operation with silicon ring modulator," Jpn. J. Appl. Phys. **51**(8R), 082101 (2012).
28. T. E. Murphy, "Design, fabrication and measurement of integrated Bragg grating optical filters," Ph.D. Thesis (Massachusetts Institute of Technology, 2001).
29. T. Okoshi, K. Kikuchi, and A. Nakayama, "Novel method for high-resolution measurement of laser output spectrum," Electron. Lett. **16**(16), 630–631 (1980).

Optics EXPRESS

30. L. E. Richter, H. I. Mandelberg, M. S. Kruger, and P. A. McGrath, "Linewidth determination from self-heterodyne measurements with subcoherence delay times," IEEE J. Quantum Electron. **22**(11), 2070–2074 (1986).
31. M. Pollnau and M. Eichhorn, "The Schawlow-Townes linewidth; a threefold approximation," in 2015 European Conference on Lasers and Electro-Optics - European Quantum Electronics Conference, (Optical Society of America, 2015), CA_P_39.
32. M. Chen, Z. Meng, J. Wang, and W. Chen, "Ultra-narrow linewidth measurement based on Voigt profile fitting," Opt. Express **23**(5), 6803–6808 (2015).
33. L. B. Mercer, "1/f frequency noise effects on self-heterodyne linewidth measurements," J. Lightwave Technol. **9**(4), 485–493 (1991).

1. Introduction

Integration of high quality ultra-narrow-linewidth lasers on a silicon photonics platform is important for several applications, including digital coherent communications, coherent LIDAR, optical metrology, and sensing [1]. Hybrid III-V silicon lasers have been shown to generate several MHz optical linewidth with phase-shifted distributed feedback (DFB) cavities [2]. To obtain a kHz linewidth laser, an external cavity can be constructed by combining the semiconductor gain medium with a Vernier-based tunable filter [3] or a high Q resonance cavity can be used with low passive loss [4]. However, these approaches generally require complex fabrication steps, or careful temperature control. Alternatively, monolithic erbium-doped aluminum oxide (Al_2O_3:Er^{3+}) lasers have been shown to achieve linewidths as low as 1.7 kHz using a DFB cavity [5]. Recently, we have demonstrated a CMOS-compatible design to integrate Al_2O_3:Er^{3+} lasers in a wafer-scale process with a single backend step [6]. The waveguide consists of a thin (~100 nm) silicon nitride (SiN_x) structure buried in a silicon dioxide (SiO_2) layer to achieve high confinement factor and mode overlap in the gain film [6–9].

In this paper, we extend the design to work for a thicker silicon nitride by using a multi-segmented waveguide structure [10–12]. This allows integration into a more general silicon photonics wafer-scale process where thicker, higher-confinement SiN_x structures might be preferred [13–15]. In addition, the design exhibits the same high confinement factor (> 85%) and a near perfect intensity overlap (> 98%) for an octave spanning range across near infrared (NIR) wavelengths (950–2000 nm).

We compare the performance of DFB lasers in discrete quarter phase shifted (QPS) cavities and distributed phase shifted (DPS) cavities [5,16]. By using a QPS-DFB configuration, we obtain single frequency lasing at 1536 nm, 1566 nm, and 1596 nm with on-chip output powers of 0.41 mW, 0.76 mW, and 0.47 mW respectively. This spans a similar emission bandwidth that has been shown previously in distributed Bragg reflector (DBR) lasers [6], covering the C and L band of the erbium gain spectrum. In a DPS cavity, we achieve an order of magnitude improvement in maximum output power (5.43 mW) for a wavelength centered at 1565 nm, corresponding to side mode suppression ratio (SMSR) of > 59.4 dB. Using a recirculating self-heterodyne delayed interferometer (R-SHDI) [17,18], we also observe a narrower linewidth for DPS-DFB at $\Delta\nu_{DPS}$ = 5.3 ± 0.3 kHz, as compared to QPS-DFB at $\Delta\nu_{QPS}$ = 30.4 ± 1.1 kHz. The improvement can be explained by reduction of spatial hole burning in the center of cavity and increased effective gain section [19,20].

Optics EXPRESS

2. Wavelength-insensitive waveguide design

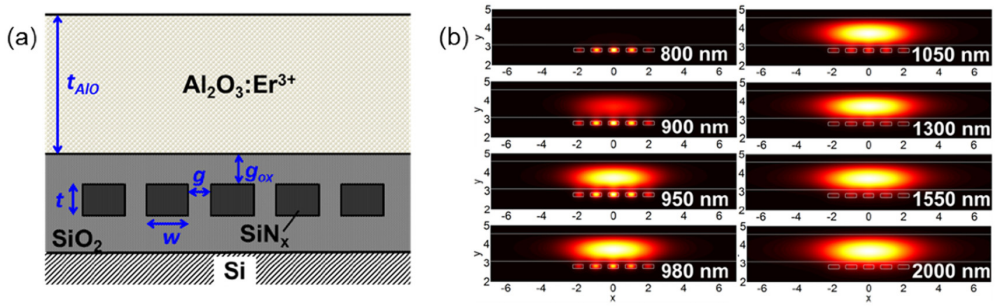

Fig. 1. (a) Schematic of wavelength-insensitive laser waveguide design by multi-segmented SiN_x structure. (b) Mode-solver calculation of the intensity distribution for various near infrared wavelengths in the multi-segmented waveguide design.

Figure 1(a) shows a schematic of the wavelength insensitive waveguide design. It consists of a silicon (Si) substrate, five SiN_x segments (thickness t of 200 nm, width w of 450 nm, and gap g of 400 nm), enclosed by a SiO_2 layer (oxide gap g_{ox} of 200 nm), and $Al_2O_3:Er^{3+}$ gain film (thickness t_{AlO} = 1100 nm). The fabrication process has been reported in references [6,21] with the only difference in the layer thickness or dopant. The distance between the Si to the bottom layer of SiN_x (>2.5μm) is sufficient to ensure the fundamental TE mode is not affected by the substrate. We use the prism coupling method to estimate the $Al_2O_3:Er^{3+}$ gain film background loss of <0.1 dB/cm and dopant concentration of 1.0×10^{20} cm^{-3} by linear fitting of measured total film loss (α_{tot}) vs. the film absorption cross-section (σ_a) around 1550 nm based on the following simplified equation:

$$\alpha_{tot} = \sigma_a N + \alpha_b$$

where σ_a is the absorption cross-section of $Al_2O_3:Er^{3+}$ film at certain wavelength, N is the doping concentration. α_{tot} and α_b are the total and background loss of the film respectively.

We perform analysis of the multi-segmented structure for a broad selection of wavelengths relevant to rare-earth emission in the NIR range; 800 nm, 900 nm, 950 nm and 980 nm (diode pump lasers for Er and Yb), 1050 nm (Yb- and Nd-doped lasers), 1300 nm (Nd-doped lasers), 1550 nm (Er-doped lasers), and 2000 nm (Tm- and Ho-doped lasers). The intensity distributions of the fundamental TE modes at the various wavelengths are calculated by a vector finite-difference 2D Eigen mode solver (in-house Matlab code), as shown in Fig. 1(b). By inspection of the modes in Fig. 1(b), we observe that the mode distribution at shorter wavelengths tends to concentrate in the silicon nitride layer. Starting from 950 nm, the mode is distributed almost exclusively in the gain layer.

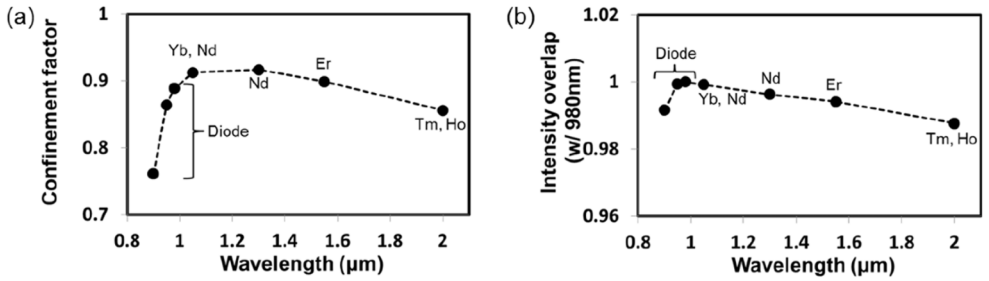

Fig. 2. (a) Calculated confinement factor in the multi-segmented waveguide for typical NIR diode pump and rare earth laser wavelengths. (b) Calculated intensity overlap between 980-nm mode and NIR diode and rare earth laser modes.

Optics EXPRESS

We define the confinement factor (γ) and overlap factor (Γ) in the active medium by the following equations:

$$\gamma_{s/p} = \frac{\int_A I_{s/p} dA}{\int_\infty I_{s/p} dA} = \frac{\sum_{gain(ij)} I_{ij}^{(s/p)}}{\sum_{ij} I_{ij}^{(s/p)}}$$

$$\Gamma_{s/p} = \frac{\int_A I_p I_s dA}{\sqrt{\int_A I_p^2 dA \int_A I_s^2 dA}} = \frac{\sum_{gain(ij)} I_{ij}^{(p)} I_{ij}^{(s)}}{\sqrt{\sum_{gain(ij)} I_{ij}^{2(p)}} \sqrt{\sum_{gain(ij)} I_{ij}^{2(s)}}},$$

where I denotes the intensity of the mode. The indicators s and p denote the signal (laser wavelength) and pump wavelength respectively. The integrals are discretized with indices i and j, and calculated by summation over each pixel in the simulation window, where the gain area A refers to Al_2O_3 layer. The confinement and overlap factors (with 980 nm chosen as a reference pump wavelength) for these wavelengths are shown in Fig. 2. We obtain >85% confinement factor for all wavelengths longer than 950 nm and >98% intensity overlap factor with a 980 nm pump mode over an octave of near-infrared wavelength light sources, demonstrating the wavelength insensitivity of the waveguide. The calculation is based on the assumption that the laser is pumped with enough power, so that it has gain over the entire waveguide mode. Therefore, the confinement factor and mode overlap are good estimations for the upper limit of the performance in the optically pumped waveguide. While here we present a design specifically optimized for 980-nm pumping, the wavelength-insensitive range and lower wavelength cutoff can also be shifted by adjusting the waveguide dimensions. In this way, the intensity overlap can be optimized to accommodate different pumping schemes, allowing the design to be used for a variety of rare earth doped lasers.

3. $Al_2O_3:Er^{3+}$ DFB lasers

We apply the five-segment wavelength-insensitive design to realize single-frequency and ultra-narrow-linewidth $Al_2O_3:Er^{3+}$ lasers. We investigate two different phase shift configurations for 2 cm long DFB cavity. In QPS-DFB, a discrete quarter phase shift is formed at the center of the cavity with a sharp frequency resonance at the Bragg wavelength. The intense electric field concentrated around the phase shifted region may limit the performance of the laser due to spatial hole burning. Alternatively, the phase shift in DPS-DFB cavity is continuously distributed in a wider region, thus improving the uniformity of the field distribution and increasing the length of the effective gain section. We compare the performance of the lasers in the following sections.

3.1 QPS-DFB

The grating unit in the QPS-DFB cavities is formed by placing additional periodic pieces on both sides of the five-segment SiN_x structure, as shown in Fig. 3(a). These periodic side pieces have width wg of 300 nm with the grating strength κ adjusted by varying the gap distance d_{wg}. We fabricated a total of 9 devices with 3 grating period variations (Λ = 482 nm, 492 nm, and 502 nm) and 3 grating strength variations (d_{wg} / κ = 600 nm / 0.6 mm^{-1}, 350 nm / 0.9 mm^{-1}, and 200 nm / 1.2 mm^{-1}).

Optics EXPRESS

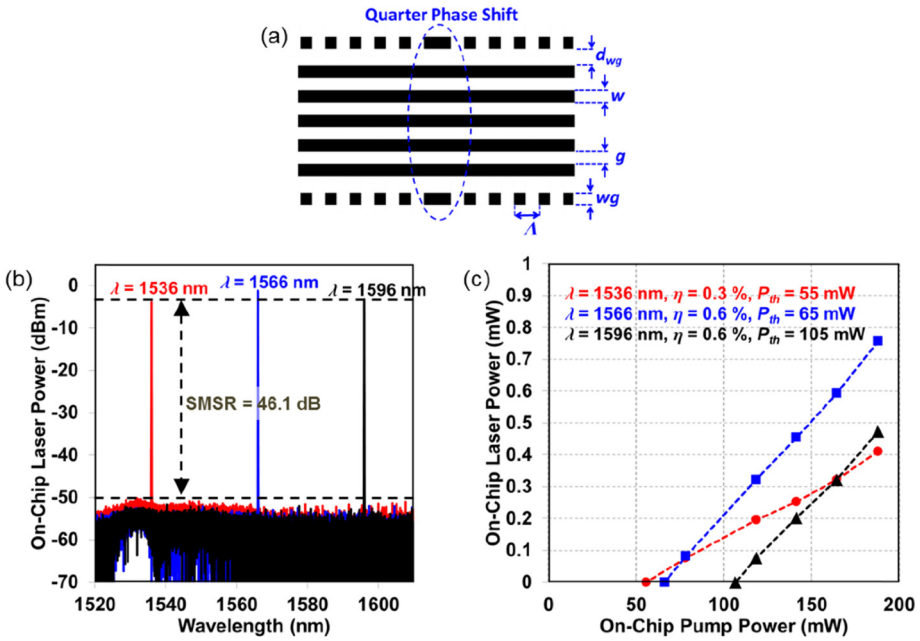

Fig. 3. (a) Design of $Al_2O_3:Er^{3+}$ QPS-DFB (not to scale). The cavity structure consists of five continuous SiN_x segments with grating perturbation provided by two additional periodic side pieces. (b) Optical spectrum of $Al_2O_3:Er^{3+}$ QPS-DFB lasers at various grating periods. (c) On-chip laser power of $Al_2O_3:Er^{3+}$ QPS-DFB lasers vs. pump power.

To characterize their performance, we pumped the DFB lasers from both sides using fiber pigtail laser diodes at 978 nm and 976 nm. We obtain the best laser performance from devices with d_{wg} = 350 nm or κ = 0.9 mm^{-1} for all three wavelengths. Figure 3(b) shows the spectra of DFB lasers operating at 1536 nm, 1566 nm, and 1596 nm, which covers a similar emission bandwidth that has been shown previously in distributed Bragg reflector (DBR) lasers [6]. The highest on-chip output power of 0.76 mW is achieved at 1566 nm. The laser operating at 1536 nm has the lowest output power, corresponding to > 46.1 dB side mode suppression ratio (SMSR) for all devices. We characterize the slope efficiency and threshold power of the lasers, as shown in Fig. 3(c). We obtain slope efficiencies η = 0.3%, 0.6%, and 0.6% and threshold powers P_{th} = 55 mW, 65 mW, and 105 mW for lasers at wavelengths 1536 nm, 1566 nm, and 1596 nm, respectively.

The thermal stability of our DFB is investigated in [22,23] showing a temperature-dependent shift of 0.02 nm/°C, which is more than two times lower than the thermal wavelength shift reported for hybrid lasers [24–27]. Such small wavelength shift is contributed by the low thermo-optic coefficients of the Al_2O_3 film and the SiN_x waveguide. The laser stability over time is mainly affected by mechanical misalignment of the fiber coupling for pump and lasing signal. A short term solution is to isolate the laser chip by covering up the test setup, so that the coupling fiber will be minimally affected by environmental fluctuations. Meanwhile, a long term solution is to integrate the diode pump onto the system so that fiber coupling is not necessary.

3.2 DPS-DFB

The DPS-DFB cavities are formed using an asymmetric design which includes a continuous segment with varying width $w_n(x)$ on one side of the waveguide and periodic pieces with spacing $d_\kappa(x)$ on the other side, where x is the axis along the cavity, as shown in Fig. 4(a). This allows accumulation of phase shift by a gradual sinusoidal change of the effective refractive index $\Delta n_{eff}(x)$ [16] while maintaining a constant grating strength κ in the phase

Optics EXPRESS

shifted region with length L_{ps}. We use the coupled mode theory [28] to determine the right combination of $w_n(x)$ and $d_\kappa(x)$ for fixed gap distance d_n = 250 nm and periodic pieces of width w_κ = 300 nm. We fabricated two different L_{ps} (0.2 cm and 0.4 cm) for grating period at 492 nm and κ = 0.7 mm^{-1}. For the 0.2-cm DPS-DFB, $w_n(x)$ varies from 168 to 351 nm and $d_\kappa(x)$ varies from 119 to 162 nm. For the 0.4-cm DPS-DFB, $w_n(x)$ varies from 168 to 271 nm and $d_\kappa(x)$ varies from 140 to 162 nm.

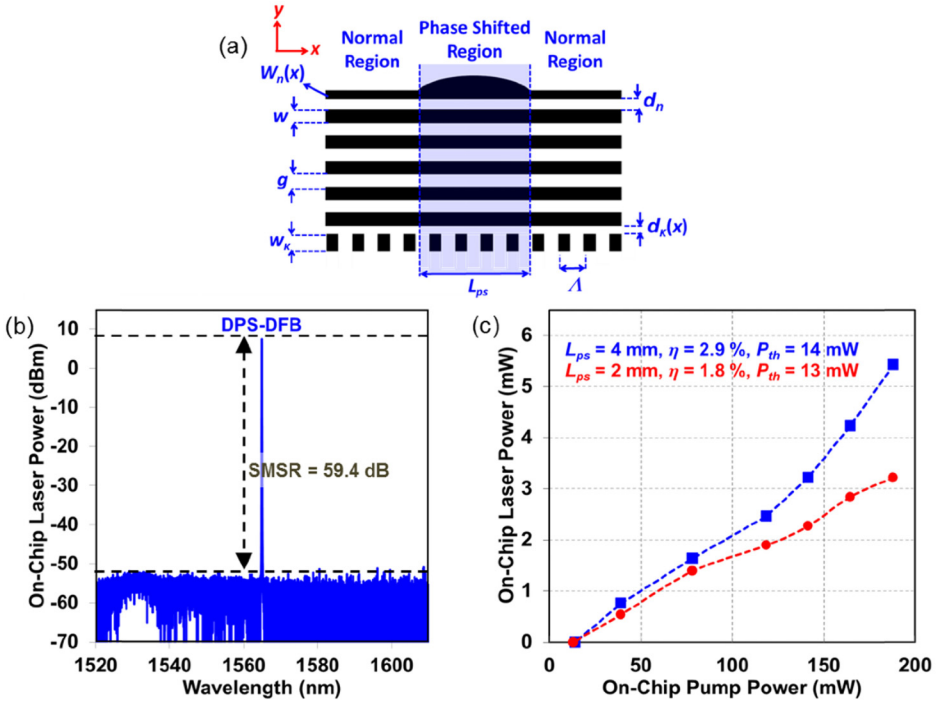

Fig. 4. (a) Design of $Al_2O_3:Er^{3+}$ DPS-DFB laser with five-segment SiN_x waveguide (not to scale). The cavity structure consists of five continuous SiN_x segments with grating perturbation provided by two additional side pieces, one with a phase shift region (top) and the other with periodic segments (bottom). (b) Optical spectrum of $Al_2O_3:Er^{3+}$ DPS-DFB lasers at various grating periods. (c) On-chip laser power of $Al_2O_3:Er^{3+}$ DPS-DFB lasers vs. pump power.

Figure 4(b) shows the spectrum of the best DPS-DFB with L_{ps} = 0.4 cm and emission centered at λ = 1565 nm. A maximum on-chip output power of 5.43 mW is obtained, corresponding to a SMSR > 59.4 dB. Figure 4(c) shows the comparison of power performance of the lasers. The longer L_{ps} DPS-DFB laser has almost double the output power at maximum pump. The threshold power is > 4 times lower than the QPS design (P_{th} = 14 mW), with close to 5 times improvement in the slope efficiency (η = 2.9%). These improvements can be attributed to a more uniform and longer active gain section in DPS-DFB. Meanwhile, compare with QPS structure, DPS structure may have slightly higher loss from (a) the asymmetry of the grating (due to transition from symmetric waveguide to asymmetric design), and (b) the tapered structure of the waveguide on a longer region that is not observed in traditional QPS. This may deviate the performance of DPS structure from theoretical expectation.

4. Ultra-narrow-linewidth measurement

For an accurate linewidth measurement in a self-heterodyne interferometer, a fiber delay length larger than the laser coherence length is required ($L_{delay} > L_{coherence}$) [29,30]. From the Schawlow-Townes formula, the fundamental (quantum) linewidth limit of an $Al_2O_3:Er^{3+}$ DFB

Optics EXPRESS

laser can reach the sub-kHz level [31]. If we assume Δv = 1 kHz and the speed of light c/n = 2 × 10^8 m/s, then the minimum L_{delay} needs to be at least 200 km. Such a long fiber requirement can be alleviated in a recirculating SHDI (R-SHDI) configuration [17,18], as shown in Fig. 5. The setup is similar to a standard SHDI, but one of the branches couples to a multipass cavity that consists of a fiber delay and an acousto optic modulator (AOM) for frequency shifting (f_{AOM} = 44 MHz). Thus, the spectrum at frequency $n \times f_{AOM}$ corresponds to an auto-correlation of the input light after passing through the equivalent delay of $n \times L_{delay}$. Lastly, an erbium doped fiber amplifier (EDFA), an optical isolator, and a tunable filter are included to compensate for roundtrip loss.

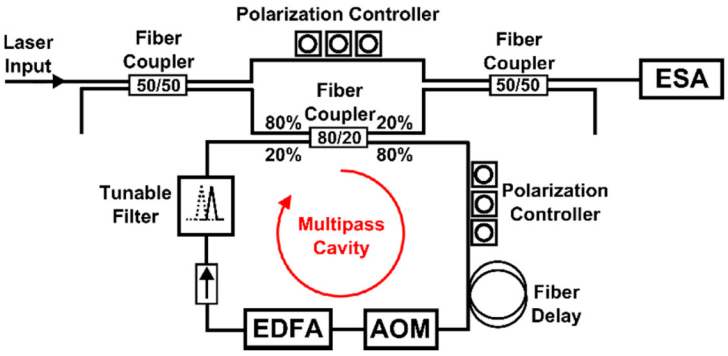

Fig. 5. Recirculating self-heterodyne delayed interferometer for ultra-narrow-linewidth measurement.

We measured the linewidth of the $Al_2O_3:Er^{3+}$ QPS-DFB laser centered at λ = 1566 nm and DPS-DFB laser centered at λ = 1565 nm, as shown in Fig. 6. For QPS-DFB laser, the spectrum was collected at a center frequency of f_c = 132 MHz (n = 3), which corresponds to a total delay length of 105 km (L_{delay} = 35 km). For the DPS-DFB laser, n = 15, f_c = 660 MHz, and the effective L_{delay} = 525 km. To differentiate the 1/f frequency noise contribution, the measured spectra are fitted with Voigt functions [32,33]. The self-heterodyne spectra are plotted around f_c with the QPS-DFB laser presented in red color and the DPS-DFB laser in blue color.

By fitting the QPS-DFB spectrum, we obtain a full width half maximum (FWHM) of the Voigt function of $FWHM_{Voigt}$ = 66.1 ± 2.5 kHz. The Voigt linewidth is further decomposed into the Gaussian component $FWHM_{Gauss}$ = 18.4 ± 7.9 kHz and Lorentzian component $FWHM_{Lorentz}$ = 60.7 ± 2.2 kHz. As the self-heterodyne measurement is an autocorrelation process whose FWHM is 2 times the laser linewidth, the optical linewidth Δv can be estimated from half the Lorentzian width of the spectrum, thus Δv_{QPS} = ½ × $FWHM_{Lorentz}$ = 30.4 ± 1.1 kHz. For the DPS-DFB laser, with the same analysis above we obtain $FWHM_{Voigt}$ = 23.8 ± 0.7 kHz, $FWHM_{Gauss}$ = 17.5 ± 1 kHz, $FWHM_{Lorentz}$ = 10.5 ± 0.5 kHz, and thus Δv_{DPS} = 5.3 ± 0.3 kHz. The linewidth improvement in the DPS-DFB laser (Δv_{QPS} = 5.73 × Δv_{DPS}) can be attributed to a higher output power and reduction in the spatial hole burning effect.

To our knowledge, this is one of the first demonstrations of a sub-10-kHz-linewidth monolithically integrated laser in a CMOS-compatible silicon photonics platform [2,3,5]. The lowest linewidth for an erbium-doped $Al_2O_3:Er^{3+}$ DFB waveguide laser was obtained in [5]. The linewidth difference between our laser and the ultra-narrow-linewidth laser reported in ref [5], might be explained by differences in the waveguide and cavity dimensions, the wavelength and linewidth quality of the pump laser and/or the mechanical and environmental stability of the experiment. By careful optimization each of these properties we expect that further reduction of the linewidth can be obtained.

Optics EXPRESS

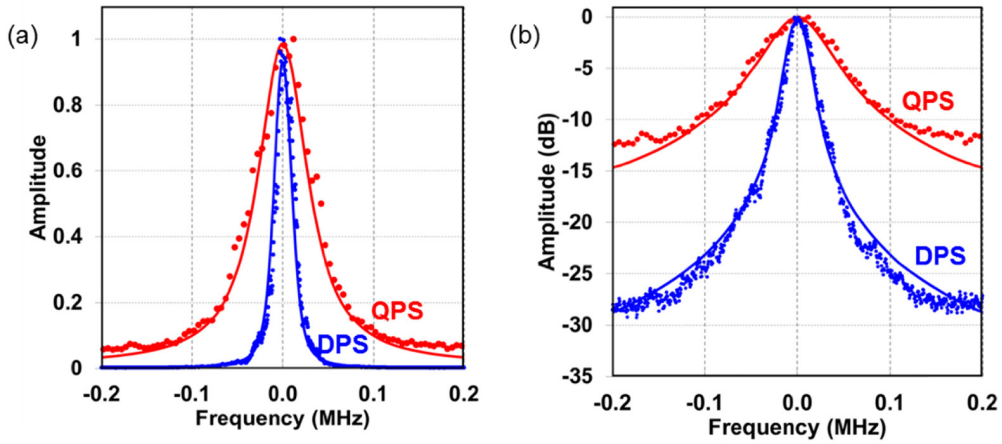

Fig. 6. Self-heterodyne spectra of $Al_2O_3:Er^{3+}$ QPS- (red) and DPS- (blue) DFB lasers in (a) linear and (b) dB scale. The solid lines of the same color are the fits of the corresponding measurements (dots).

5. Conclusion

We demonstrate narrow linewidth $Al_2O_3:Er^{3+}$ DFB lasers using a multi-segmented SiN_x silicon-compatible waveguide design. The waveguide design has > 85% confinement factor and > 98% intensity overlap at wavelengths from 950 to 2000 nm, showing octave-spanning wavelength-insensitivity in the NIR range and enabling efficient pumping at broadly-spaced pump and signal/laser wavelengths. We apply the design to QPS-DFB and DPS-DFB cavities. In the QPS-DFB configuration, we obtain maximum output powers of 0.41 mW, 0.76 mW, and 0.47 mW at widely spaced wavelengths within both the C and L bands of the erbium gain spectrum (1536 nm, 1566 nm, and 1596 nm). In a DPS cavity, we achieve an order of magnitude improvement in maximum output power (5.43 mW) for a wavelength centered at 1565 nm, corresponding to a side mode suppression ratio (SMSR) of > 59.4 dB. Finally, we measure the optical linewidths with an R-SHDI setup to obtain $\Delta\nu_{QPS}$ = 30.4 ± 1.1 kHz and $\Delta\nu_{DPS}$ = 5.3 ± 0.3 kHz. The overall improvement of the DPS-DFB cavity can be attributed to the reduction of spatial hole burning in QPS-DFB cavity and a longer effective gain section. Even narrower linewidth can be achieved by mechanical stabilization of the setup, increasing the pump absorption efficiency, increasing the output power, or enhancing the cavity Q. The Q can be enhanced by accounting for $Al_2O_3:Er^{3+}$ film thickness variation across the cavity, reducing the SiN_x loss and optimizing the DFB grating strength.

Funding

Defense Advanced Research Projects Agency (DARPA) E-PHI (grant no. HR0011-12-2-0007) project.

Acknowledgment

The authors would like to acknowledge Prof. Markus Pollnau, Dr. Edward Bernhardi and Dr. Joshua Conway for the helpful discussions. N. Li acknowledges a fellowship from the Agency of Science, Technology and Research (A*STAR), Singapore.